JCTC Journal of Chemical Theory and Computation

Article

pubs.acs.org/JCTC

Generalized Langevin Methods for Calculating Transmembrane Diffusivity

Kari Gaalswyk, Ernest Awoonor-Williams, and Christopher N. Rowley*

Department of Chemistry, Memorial University of Newfoundland, St. John's, NL A1B 3X9, Canada

Supporting Information

ABSTRACT: The membrane permeability coefficient of a solute can be estimated using the solubility–diffusion model. This model requires the diffusivity profile ($D(z)$) of the solute as it moves along the transmembrane axis, z. The generalized Langevin equation provides one strategy for calculating position-dependent diffusivity from straightforward molecular dynamics simulations where the solute is restrained to a series of positions on the z-coordinate by a harmonic potential. The diffusivity of the solute is calculated from its correlation functions, which are related to the friction experienced by the solute. Roux and Hummer have derived expressions for the diffusion coefficient from the velocity autocorrelation function (VACF) and position autocorrelation function (PACF), respectively. In this work, these methods are validated by calculating the diffusivity of H_2O and O_2 in homogeneous liquids. These methods are then used to calculate transmembrane diffusivity profiles. The VACF method is less sensitive to thermostat forces and has incrementally lower errors but is more sensitive to the spring constant of the harmonic restraint. For the permeation of a solute through a lipid bilayer, the diffusion coefficients calculated using these methods provided significantly different results. Long-lived correlations of the restrained solute due to inhomogeneities in the bilayer can result in spuriously low diffusivity when using the PACF method. The method based on the VACF does not have this issue and predicts higher rates of diffusion inside the bilayer.

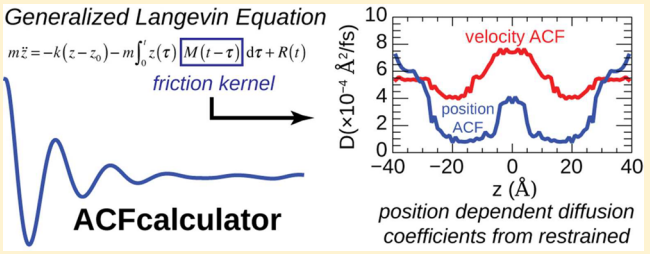

INTRODUCTION

The rate of diffusion of a solute is fundamental to biochemical transport processes such as protein–ligand binding[1,2] and membrane permeation.[3,4] The diffusivity of a solute is particularly significant to the permeation of solutes through lipid bilayer membranes. In the inhomogeneous solubility–diffusion model,[5−9] the permeability of a small-molecule solute can be estimated from the potential of mean force ($w(z)$) and the diffusion coefficients ($D(z)$) of the solute as a function of its position along the transmembrane axis (z). In this model, the permeability coefficient (P_m) can be expressed as an integral over an interval of z that spans the bilayer.

$$\frac{1}{P_m} = \int_{z_1}^{z_2} \frac{e^{w(z)/k_B T}}{D(z)} dz \quad (1)$$

There are several mature methods for calculating $w(z)$ using molecular simulations,[8,10−12] but the calculation of the $D(z)$ profile has received less attention. The Einstein[13] or Kubo[14] relations can be used to calculate the diffusion coefficient of a solute in a homogeneous solution by analysis of a molecular dynamics (MD) trajectory, but these methods have limited applicability for inhomogeneous systems such as a bilayer. In these systems, the variation of the solute diffusivity is large because the frictional environment varies dramatically as the solute moves from bulk water, through the interface, and into the membrane interior.

The fluctuation–dissipation equation provides one method to calculate the diffusion coefficient from the autocorrelation function of the force exerted on a solute constrained at a point along the reaction coordinate.[14] This method requires the imposition of a constraint on the z-position of the solute and the calculation of the force autocorrelation function. This autocorrelation function can be difficult to calculate accurately. More elaborate statistical techniques have also been developed to interpret diffusion coefficients from MD simulations,[15−18] although implementing and applying these methods can be an involved process.

The generalized Langevin equation (GLE) provides straightforward and practical methods for calculating diffusion coefficients. In general terms, if a degree of freedom of a system is restrained using a harmonic potential, its motion can be described by the GLE solution for a harmonic oscillator in a frictional bath. The diffusivity along this coordinate of the solute can then be calculated by analysis of this trajectory. Roux and co-workers developed techniques to calculate these properties from the velocity autocorrelation function (VACF).[19−21] Hummer later derived a simplified expression to calculate $D(z)$ from the position autocorrelation function (PACF).[15] Although the PACF-based method has been used to calculate $D(z)$ in several membrane permeation studies,[22−24]

Received: July 26, 2016
Published: September 27, 2016

DOI: 10.1021/acs.jctc.6b00747
J. Chem. Theory Comput. 2016, 12, 5609−5619

Lee et al. showed that there are some practical issues associated with this method.[8]

In this paper, we present a comparison of these GLE-based methods for calculating the diffusivity of small molecule solutes in various liquids and with various simulation conditions. A general, automatic method for the calculation of the diffusion from the VACF is developed. The diffusivity profile of a water molecule across a lipid bilayer is calculated using the PACF and VACF methods.

THEORY AND METHODS

GLE Methods for Calculating Diffusion Coefficients. The basic procedure for calculating a diffusion coefficient using a GLE method is to restrain the position of the solute using a harmonic potential. For the purpose of this paper, we will consider motion along the z-coordinate.

The GLE for the motion of a harmonic oscillator along the z-coordinate takes the form

$$m\ddot{z}(t) = -kz(t) - \int_0^t \dot{z}(\tau)\zeta(t-\tau)\mathrm{d}\tau + R(t) \tag{2}$$

Here, k is the spring constant of the oscillator, $\zeta(t)$ is the dynamic friction kernel (or memory kernel), $\dot{z}$ is the velocity of the system along the z-coordinate, and $R(t)$ is the random force.

The effect of the balance of the system (i.e., the solution and the bilayer) on the oscillator is introduced through the friction and random force terms. The analytical solutions for the PACF ($C_z(t)$) and VACF ($C_v(t)$) of a harmonic oscillator in a dissipative bath are both oscillatory functions that decay exponentially with time.[25] The rate of decay depends on the friction coefficient of the dissipative forces that the solute experiences from its surroundings. The autocorrelation functions of a harmonically restrained solute in a condensed phase calculated numerically from an MD simulation are generally consistent with this form; for example, Figure 1 shows the PACF and VACF of a harmonically restrained water molecule in liquid hexane calculated from a molecular dynamics simulation. Although these functions are generally oscillatory, the oscillations are not always apparent if the rate of decay is high.

These autocorrelation functions provide a connection between the dynamics of a restrained solute and the friction it experiences from the solvent. Extending the work of Straub and Berne,[26] Roux and co-workers derived an expression for the diffusion coefficient of the solute from the GLE of a harmonic oscillator:[19−21]

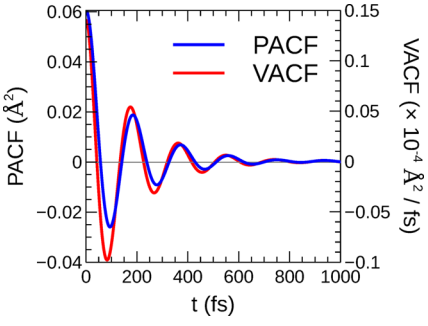

Figure 1. Position and velocity autocorrelation functions of a H_2O molecule in liquid hexane restrained with a harmonic potential. For this system, both functions are exponentially decaying oscillatory functions.

$$D(z_i = \langle z\rangle_i) = \lim_{s\to 0} \frac{-\hat{C}_v(s; z_i)\langle \delta z^2\rangle_i \langle \dot{z}^2\rangle_i}{\hat{C}_v(s; z_i)[s\langle \delta z^2\rangle_i + \langle \dot{z}\rangle_i/s] - \langle \delta z^2\rangle_i \langle \dot{z}^2\rangle_i} \tag{3}$$

δz is the displacement of the position, z, from its average value. $\langle z^2\rangle$ and $\langle \dot{z}^2\rangle$ are the variances of the position and velocity of the oscillator, respectively. $\hat{C}_v$ is the Laplace transform of the velocity autocorrelation function. The diffusion coefficient is the limit of this equation as $s \to 0$, where s is the coefficient of the Laplace transform. This limit cannot be taken directly because of a singularity at $s = 0$, so the limit must be extrapolated from $D(s)$ in the range where the function is well-behaved.

Hummer derived a simpler form of this equation that uses the PACF instead of the VACF:[15]

$$D(z_i = \langle z\rangle_i) = \frac{\mathrm{var}(z)^2}{\int_0^\infty C_z(t)\mathrm{d}t} \tag{4}$$

An advantage of this form is that is it not necessary to store the velocity time series, compute a Laplace transform, or perform the extrapolation step; the diffusion coefficient can be calculated in a straightforward way from the variance and PACF alone. The derivation of these expressions from the GLE is presented in Appendix A.

Practical Calculation of Correlation Functions. Both the PACF and VACF methods for calculating the diffusion coefficients require the calculation of a correlation function for the motion of the solute when the solute is restrained to some position along the transmembrane coordinate (z) by a harmonic potential:

$$\mathcal{V}(z) = \frac{1}{2}k(z - z_0)^2 \tag{5}$$

where k is the spring constant of the restraint and z_0 is the reference position. The diffusion coefficient can be calculated at different positions along the coordinate by selecting different reference positions for the restraining harmonic potential.

Beginning from an equilibrium configuration for the membrane system, a time series of the z-coordinate of the center of mass of the solute is collected by performing an MD simulation. The simulation must be sufficiently long for the correlation functions to be calculated with high accuracy. This typically requires a simulation that is at least 1 ns in length. These simulations are performed with restraint reference positions at intervals that span the membrane (e.g., $z_0 = -40$, -39, ..., 0, ..., 39, 40 Å).

The time series of the displacement of the solute, δz, or the velocity along the z-coordinate, $\dot{z}$, can be used to calculate the position or velocity autocorrelation functions, respectively. The correlation functions for a time series with regularly spaced intervals can be calculated most directly by a summation over the trajectory:[27]

$$C_z(t) = \langle \delta z(0)\delta z(t)\rangle = \frac{1}{n_{\mathrm{samples}}} \sum_{i=0}^{n_{\mathrm{samples}}} \delta z(i)\delta z(t+i) \tag{6}$$

where $\delta z(t) = z(t) - \langle z\rangle$.

Because these correlation functions should converge to zero after the relaxation time of the system, it is generally sufficient

DOI: 10.1021/acs.jctc.6b00747
J. Chem. Theory Comput. 2016, 12, 5609−5619

to calculate the correlation function over a short interval (e.g., 0−5 ps). For a particularly long time series, the correlation functions could also be calculated more efficiently using Fourier transforms,[28,29] so the computational cost for the calculation of the correlation functions will be modest even for long time series.

These GLE-based methods are attractive for calculating transmembrane diffusivity because many biomolecular simulation codes (e.g., NAMD and GROMACS) natively support the imposition of a harmonic restraint such as eq 5 and for the time series generated by this simulation to be saved to disk. This procedure is identical to that used to perform an umbrella sampling simulation to calculate the potential of mean force for the permeation of a solute. In principle, both properties could be calculated from the same data, although in practice there are some issues regarding this method (see below).

Practical Calculation of Diffusion from VACF. Calculation of $D(z)$ using the VACF-based method requires a method to find the limit as $s \to 0$ in eq 3. The limit cannot be taken directly due to a singularity at $s = 0$. There are two additional singularities in $D(s)$, and the function is only well-behaved in the interval between them, so the value of $D(s = 0)$ must be extrapolated from the range between the second and third singularities (Figure 2). To facilitate routine calculation of

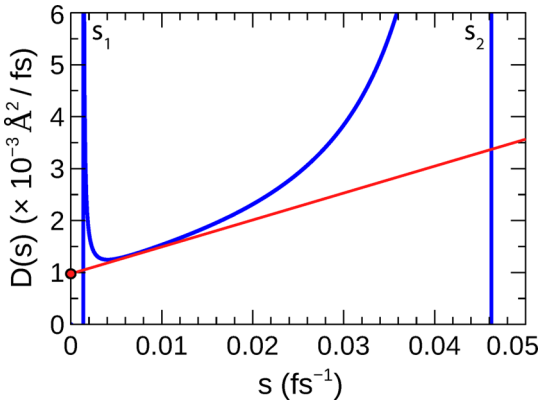

Figure 2. $D(s)$ curve (eq 3) for a harmonically restrained O_2 molecule in liquid hexane. The diffusion coefficient ($D(s = 0) = 1.04 \times 10^{-3}$ Å^2 fs^{-1}) is estimated by linearly extrapolating $D(s)$ from the region of lowest curvature between singularities s_1 and s_2.

$D(z)$ using the VACF method, we developed an algorithm to extrapolate $D(z, s = 0)$ from $D(z, s)$. The full details of the algorithm are described in Appendix B.

Technical Details of the Simulations. *Simulations of Bulk Liquids.* MD simulations of the solutes in the homogeneous solvents were performed using NAMD 2.10.[30] The SHAKE algorithm was used to constrain bonds containing hydrogen.[31] Lennard-Jones interactions were truncated at 12 Å using a switching function in the 10−12 Å interval. A Langevin thermostat at 298.15 K with a damping coefficient of 1 ps^{-1} was used for equilibration. The time series for the calculation of the diffusion coefficients using the GLE-based methods were performed under microcanonical (NVE) conditions. The simulation time step was 2 fs. The electrostatic interactions were calculated using the particle mesh Ewald (PME) method with a 32 × 32 × 32 grid.[32] Diffusion coefficients were calculated from the average of three trajectories. For each simulation, a 1 ns MD simulation was performed under isothermal−isobaric (NpT) conditions to equilibrate the system before a 10 ns production simulation was performed under NVE conditions. To calculate the diffusion coefficient using the GLE-based methods, a harmonic restraint along the z-axis was imposed on the center of mass of the solute with a spring constant of 10 kcal mol^{-1} Å^{-2}.

The force field of Fischer and Lago was used in simulations of O_2.[33] The CHARMM-modified TIP3P model was used in the simulations involving water.[34,35] The CHARMM general force field was used to describe the aliphatic solvents.[36]

Lipid Bilayer Simulations. The simulation cell contained 64 DPPC lipids arranged in a symmetric bilayer parallel to the XY-plane. The lipids were represented using the CHARMM36 lipid force field.[37] The bilayer was surrounded by a solvent layer containing 4551 TIP3P-model water molecules. The dimensions of the simulation cell were roughly 44 × 44 × 114 Å.

A 40 ns steered MD simulation was performed to generate the initial configurations for the restrained simulations. Over the course of this simulation, a water molecule from solution (z = 40 Å) was pulled along the z-axis to the center of the bilayer (z = 0 Å), while a second water molecule was pulled from the center of the bilayer to the opposing side of the bilayer (z = −40 Å). Configurations were selected at 1 Å separations relative to the center of mass of the bilayer, spanning a −40 to 40 Å interval.

The permeating water molecules were restrained to their reference positions using a harmonic restraint with a 30 kcal mol^{-1} Å^{-2} spring constant to ensure the simulations sampled a point close to the reference position (i.e., $\langle z \rangle \approx z_0$) given the significant curvature of the underlying PMF.[38] These restrained simulations were equilibrated by performing a 10 ns MD simulation. The time series used to calculate the $D(z)$ profiles were calculated from 2 ns MD simulations in the microcanonical ensemble. To generate distinct starting points for the successive series, the system was equilibrated for 2 ns. The profiles presented in Figure 6 are calculated from the average of these three simulations, symmetrized about the center of the bilayer. The temperature of the system was 315 K. The center of mass of the bilayer was restrained to z = 0 Å using a 5 kcal mol^{-1} Å^{-2} spring constant.

The unrestrained simulations of the water molecule diffusing at the center of the bilayer were equilibrated by running 1 ns simulations where the permeating water was restrained to the center of the bilayer. A 5 ps microcanonical simulation was initiated from the equilibrated structure. This equilibration and sampling procedure was repeated 2500 times to generate the distribution plotted in Figure 7.

Numerical Methods. The calculation of the solute diffusivity using the PACF and VACF GLE methods from MD time series has been implemented in our code, ACF-Calculator,[39] which is freely available under the GNU public license. This program can read time series files generated from CHARMM, NAMD, and GROMACS as well as generic delimiter-separated files. In the work presented here, the correlation functions were calculated over the 0−4 ps interval by direct summation. No cutoff was used in the numerical integration of the correlation functions.

RESULTS AND DISCUSSION

Validation of GLE Methods with Homogeneous Liquids. Benchmark calculations were performed to assess the accuracy of the GLE methods for calculating the diffusivity of solutes in membrane-like environments. The diffusivities of H_2O and O_2 molecules in bulk liquids of water (TIP3P model),

DOI: 10.1021/acs.jctc.6b00747
J. Chem. Theory Comput. 2016, 12, 5609−5619

pentane, and hexane were calculated using the PACF and VACF GLE methods. For these homogeneous solutions, the diffusivity of the solute can also be calculated by performing a long, unrestrained simulation. The mean square displacement of the solute can be related to the diffusivity using the Einstein relation:

$$D = \frac{1}{6t}\langle |r(t) - r(0)|^2 \rangle \tag{7}$$

For these homogeneous solutions where there is no position dependence to the diffusivity, the Einstein relation provides independent and rigorous values to compare the GLE methods to. The diffusivities calculated using these three methods are compared in Figure 3.

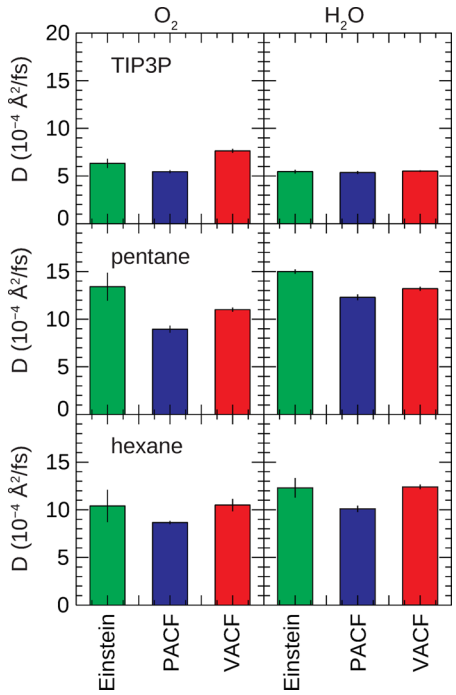

Figure 3. Diffusivity of O_2 (left) and H_2O (right) in liquid water (TIP3P model), pentane, and hexane calculated by the PACF and VACF GLE methods. For comparison, the diffusivities calculated using the Einstein relation are also shown.

Both GLE methods are reasonably effective for calculating the diffusivity of these solutes in both aqueous and paraffinic solutions. Generally, all three methods yield comparable values, although the VACF method is generally in closer agreement with the Einstein relation and has the smallest standard deviation of all three methods; the χ^2 values for the PACF and VACF-calculated diffusion coefficients relative to the average Einstein diffusion coefficient are 10.3 and 2.5 cm^2/s, respectively.

Effect of Thermostat Friction of Calculated Diffusivity. MD simulations are often performed using stochastic thermostats. For example, a Langevin thermostat can be used to sample the canonical ensemble (NVT) of the system by applying artificial frictional and random forces to the atoms of the system.[40] These forces change the dynamics of the molecules, so transport properties such as diffusion will be affected.[41,42] To assess the effect of a thermostat on the diffusivities calculated with the GLE methods, the self-diffusion coefficient of TIP3P-model water was calculated from simulations with a Langevin thermostat and friction coefficients in the range commonly used in biomolecular MD simulations (γ = 1−10 ps^{-1}). We compare this to the diffusion coefficients calculated from a NVE MD simulation, where no thermostat forces are applied, and from an NVT MD simulation using a Lowe−Andersen thermostat,[43] which is a stochastic thermostat that has a smaller effect on diffusion coefficients.[44,45] The diffusivity of TIP3P-model water calculated using these methods is presented Figure 4.

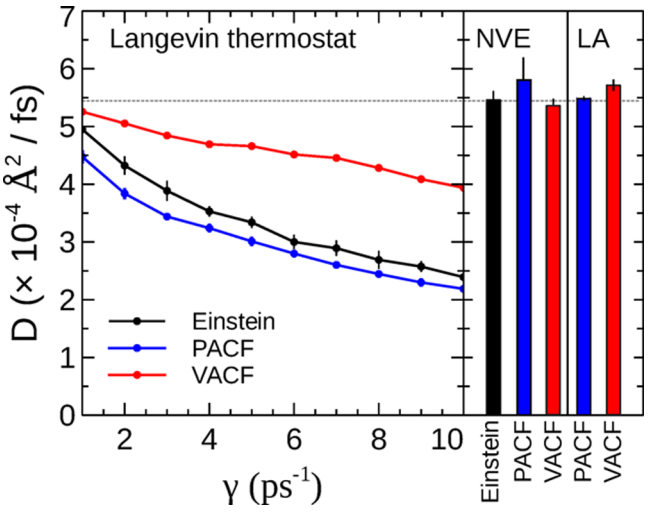

Figure 4. Effect of the Langevin thermostat frictional coefficients (γ) on the diffusivity of TIP3P-model water (left). The diffusivity calculated with the PACF, VACF, and Einstein methods all decrease as the friction coefficient of the Langevin thermostat is increased. The reference values for a simulation performed under NVE conditions (i.e., no thermostat) and those performed using a Lowe−Andersen thermostat (LA) are shown for comparison (right). The dotted line indicates the diffusivity calculated using the Einstein relation and the NVE simulation.

Both the PACF and VACF methods show a decline in the diffusion coefficient as the thermostat frequency is increased. This can be attributed to the damping of the dynamics of the oscillating solute due to the frictional force imposed by the thermostat. The PACF method is more sensitive to this effect; the diffusivity calculated using the PACF method drops to from a value of 5.8 × 10^{-4} $Å^2$/fs when no thermostat is applied to a value of 2.2 × 10^{-4} $Å^2$/fs when a thermostat coefficient of γ = 10 ps^{-1} is used. This decline is similar to the decrease in diffusivity observed when the Einstein relation is used. In comparison, the diffusivity drops to only 4.0 × 10^{-4} $Å^2$/fs when γ = 10 ps^{-1} with the VACF method. This difference is due to the application of the Laplace transform in the VACF method, which reduces the influence of the correlation function for large values of t. The thermostat forces have a larger effect on the correlation functions at larger values of t because the dynamics have been damped and randomly perturbed by these forces for a longer period.

Simulations used to calculate the potential of mean force must use a thermostat to sample the correct ensemble for the system they are describing. If the same simulations are to be used to calculate $D(z)$ as are used to calculate $w(z)$, it is important to use a small frictional coefficient or to use a thermostat that does not have a large effect on diffusivity (e.g., Nosé−Hoover or Lowe−Andersen).

Effect of Restraint Spring Constant on Calculated Diffusivity. Several factors affect the choice of the spring

DOI: 10.1021/acs.jctc.6b00747
J. Chem. Theory Comput. 2016, 12, 5609−5619

constant of the harmonic restraint potential on the solute in the simulations for the GLE diffusivity calculations. The assumption underlying these GLE-based methods is that the dynamics of the solute can be described as a harmonic oscillator in a dissipative bath.[46] In heterogeneous environments such as a lipid bilayer, the underlying free energy surface can be rough, so the harmonic restraining force should be considerably stronger than these "bath" forces. Likewise, to calculate a diffusion coefficient at an arbitrary point along this coordinate, the restraining force must be sufficiently large so that the average position along the coordinate is close to the reference position (e.g., $\langle z \rangle_i \approx z_{0,i}$).

To test for systematic errors that could result from the choice of the spring constants, simulations were performed to calculate the self-diffusivity of water using the GLE-based methods with spring constants ranging from 1 to 50 kcal mol^{-1} Å^{-2} (Figure 5a). The PACF method shows some variation with

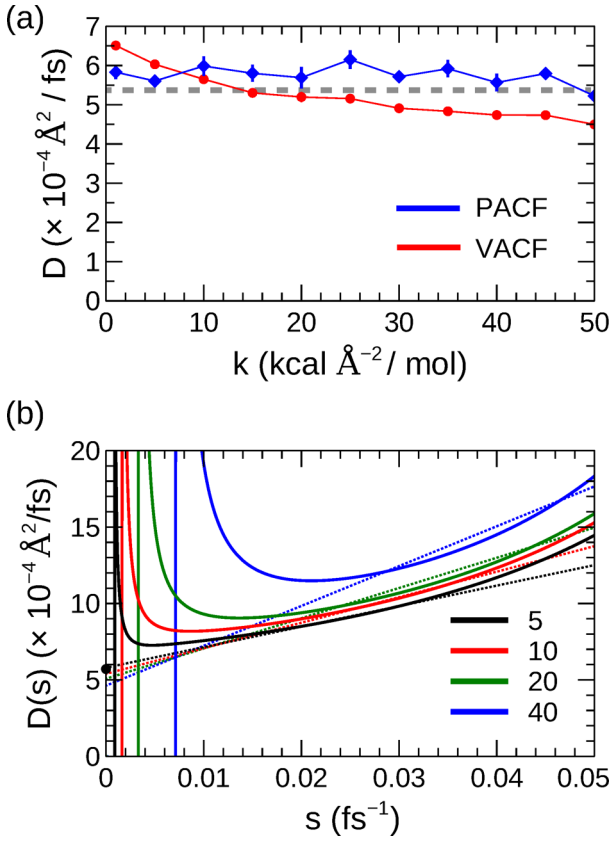

Figure 5. (a) The diffusivity of TIP3P-model water calculated using the GLE methods with various spring constants for the harmonic restraining force (k). The diffusivity calculated using the Einstein relation is indicated by the dashed gray line. (b) The $D(s)$ profiles calculated using the VACF method (eq 3), corresponding to select values of the spring constant, k. The dotted lines indicate the extrapolation. The reference diffusion coefficient is indicated by a black dot on the y-axis. Note that the dotted lines are not necessarily tangent to the $D(s)$ curves because the extrapolation is performed over a segment to improve numerical stability (see Appendix B).

the spring constant, but there is no systematic trend, and all simulations performed with the various spring constants give a prediction in reasonable agreement with the diffusivity calculated using the Einstein relation.

The VACF method varies more significantly with the spring constant. This can be understood by comparing the $D(s)$ curves calculated with different spring constants (Figure 5b). The spring constant affects both the variance of the simulation and the Laplace transform of the VACF of eq 3, causing $D(s)$ to change with k. Although formally it should be possible to calculate D using eq 3 with any value of k, the need to extrapolate $D(s)$ introduces a sensitivity to k. One measure of the reliability of the extrapolation can be assessed by the coefficient of determination for the linear fit. In these tests, $r^2 > 0.99$ was generally achieved when D was predicted accurately.

Transmembrane Diffusivity Profiles. To compare these methods for calculating the diffusivity of solutes permeating through a lipid bilayer, simulations were performed where a water molecule was restrained at positions that span the bilayer in the interval $z = [-40, 40$ Å$]$ along the transmembrane axis. These profiles are presented in Figure 6.

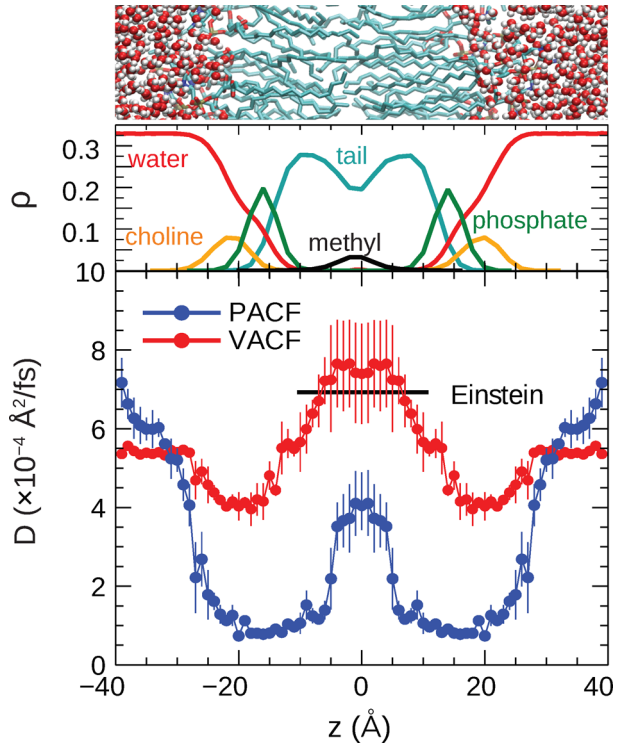

Figure 6. Diffusion coefficients of a water molecule permeating through a DPPC lipid bilayer calculated using the PACF and VACF GLE methods. The upper panel shows the density contribution of the various membrane components in the bilayer. The VACF method predicts systematically higher rates of diffusion inside the bilayer. The profiles are symmetrized about the center of the bilayer. Error bars were calculated from the standard deviations of the three independent simulations. The diffusivity at the center of the bilayer calculated using the Einstein density method is indicated by the black line.

The PACF and VACF methods predict similar diffusion coefficients in solution ($|z| > 35$ Å), although the diffusivity calculated with the VACF method is unaffected until the solute is immersed in the headgroups, while the PACF method indicates a decline that begins in the solution above the bilayer. Inspection of the correlation functions in this interval show that the PACF has greater correlation in the 500−1000 fs range for the simulations near the bilayer interface, although this is not present in the VACF (see the Supporting Information). The statistical noise for the PACF is greater than for the VACF, even in solution, so the uncertainty of the PACF calculations are much larger in this regime. We note that diffusivity in the

DOI: 10.1021/acs.jctc.6b00747
J. Chem. Theory Comput. 2016, 12, 5609−5619

solution is anomalously high because the TIP3P water model overestimates the diffusivity of water.[47]

There are more significant differences in the diffusivity inside the bilayer. The PACF method predicts diffusivities that are less than 1×10^{-4} Å^2/fs in the upper regions of the lipid tails (5 Å < |z| < 20 Å). Both methods predict relatively high diffusivities in the disordered region at the center of the bilayer (|z| < 5 Å), although the VACF method predicts higher diffusivities (4×10^{-4} and 8×10^{-4} Å^2/fs, respectively).

The diffusivity at the center of the bilayer can also be calculated by unrestrained molecular dynamics simulations, which provide a test that is independent of the GLE model. A series of unrestrained MD simulations was performed by restraining the solute to the center of the bilayer then releasing the restraint and saving the trajectory for a short interval (e.g., 5 ps). Because $w(z)$ of a permeating water molecule is essentially flat at the center of the bilayer,[9,24] the dynamics of the solute can be described as being Brownian. The Einstein relation for probabilities relates the standard deviation of the density distribution at time t to the diffusion coefficient:

$$\rho(z, t) = \frac{N}{\sqrt{4\pi D t}} \exp\left(\frac{-z^2}{4Dt}\right) \quad (8)$$

From the standard deviation of 2500 trajectories initiated from the center of the bilayer, the diffusion coefficient is estimated to be 6.9×10^{-4} Å^2/fs (Figure 7). This indicates that the diffusivity

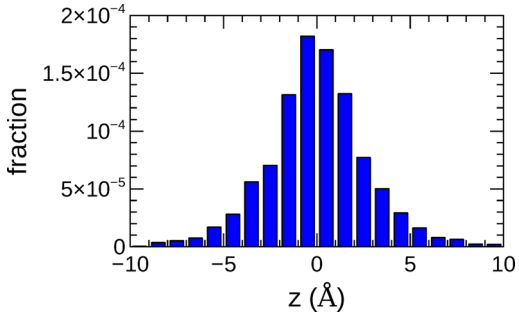

Figure 7. Histogram for the displacement of a water molecule at the center of the bilayer (z = 0 Å) along the z-axis after 5 ps.

inside the bilayer is overestimated by the VACF method but is considerably higher than that predicted by the PACF method. This is consistent with estimates by Comer et. al.[48] Experimental electron paramagnetic resonance (EPR) studies of NO permeation through a lipid bilayer also indicate that the diffusivity of a small-molecule solute is elevated in the interior of a bilayer.

Slow Decay of the PACF. One potential cause for the difference between the PACF and VACF diffusion profiles is apparent in the correlation functions used to calculate the diffusivities. Lee et al. showed that the PACF of a solute restrained inside a lipid bilayer with a harmonic potential can decay far slower than those in bulk liquids.[8] In some cases, the PACF can have a significantly nonzero value even after 5 ps. Formally, the denominator of eq 4 should be integrated until $C_z(t)$ converges to zero, although in practice, it is typically only computed for some predefined interval. This causes the calculated diffusion coefficient to become sensitive to the bounds chosen for the integration. The diffusion coefficients calculated using eq 4 can decline to very low values (i.e., $D < 1 \times 10^{-4}$ Å^2/fs) at bilayer depths where the PACF decays slowly.

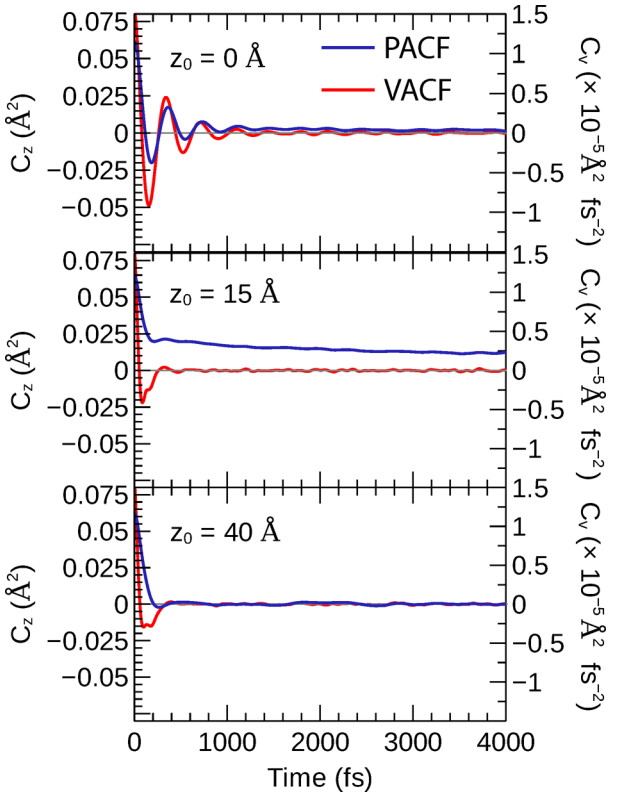

Figure 8. Position and velocity autocorrelation functions of a water molecule restrained at different depths in a DPPC bilayer (blue and red, respectively). The PACF converges to zero in less than 1000 fs when the solute is in the bulk solution (z_0 = 40 Å) but does not converge to zero even after 4 ps when the solute is immersed in the bilayer (z_0 = 0 and 15 Å) The VACF is plotted on the secondary axis. The VACF converges to zero within 1000 fs for all solute depths.

This slow decay is apparent in the PACFs of a water molecule restrained at different reference positions along the z-axis of a DPPC lipid bilayer system (Figure 8). When the solute is in the bulk liquid of water above the bilayer (z_0 = 40 Å), the PACF converges to zero in less than 1000 fs. The PACF holds a significant nonzero value when the solute is immersed in the bilayer. This effect is apparent in the simulation where the solute is at the center of the bilayer (z_0 = 0 Å) but is most severe when the solute is in the water−lipid interfacial region (z_0 = 15 Å).

The PACF indicates that there is a degree of correlation in the position of the solute after an elapsed time. In most bulk liquids, the frictional forces are sufficiently strong so that the position of the restrained solute is no longer correlated after 1−2 ps (i.e., its current position is independent of its previous). The long tails on the PACFs for simulations inside the bilayer, such as the z_0 = 0 and 15 Å plots in Figure 1, indicate that the position of the solute can have significant correlations for much longer intervals than those in bulk liquids (e.g., z_0 = 40 Å).

These long time scale correlations are apparent in the time series of a simulation of a water molecule restrained inside the bilayer at z_0 = 10 Å (Figure 9). Analysis of the time series shows fluctuations that can extend over 100 ps. These long time scale fluctuations can be attributed to slow rearrangements of the bilayer that hinder the oscillation of the solute and the changes in the hydration state of hydrogen-bonding solutes. The GLE methods rely on the description of the dynamics of the restrained solute as a harmonic oscillator in a frictional bath, so these inhomogeneities violate an assumption of the model. This type

DOI: 10.1021/acs.jctc.6b00747
J. Chem. Theory Comput. 2016, 12, 5609−5619

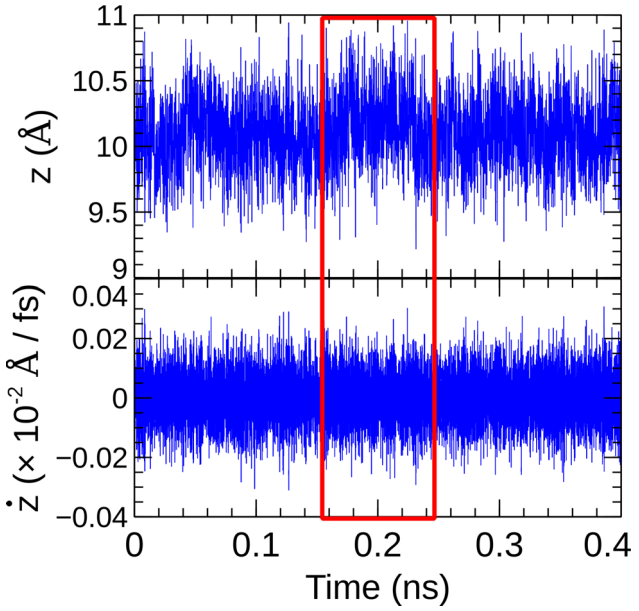

Figure 9. The time series (top) and velocity series (bottom) of a water molecule restrained to oscillate around z = 10 Å with respect to the center of a DPPC bilayer by a harmonic potential. Fluctuations in the position occur with a lifetime on the order of 0.1 ns during this 0.4 ns simulation.

of long time scale correlation of the position of a solute restrained inside a lipid bilayer has been previously noted by Neale et al. as a challenge in calculating the potential of mean force ($w(z)$) of solute permeation.[12,49,50]

The VACF does not exhibit the same slow decay. The VACF converges to zero in less than 2000 fs for all reference positions, including the solution, interface, and bilayer center. In the lipid tail region (z_0 = 0 Å), the PACF decays to only 10% of its initial value after 4 ps, while the VACF decays to a value near 0 after only 500 fs. Physically, the VACF does not show long-term correlations because even if a long time scale fluctuation occurs in the position of the solute, the oscillations in the velocity of the solute are not strongly affected. This is apparent in the lower panel of Figure 9, which shows the velocity time series of the same simulation. This suggests that the VACF-based method to calculate $D(z)$ could resolve the issues related to the slow decay that affect the PACF-based method.

The long time scale decay in the PACF and large standard deviations of the diffusivities calculated using both of these GLE methods reflect the heterogeneity of the environment of a solute inside the bilayer. Previous simulation studies have demonstrated that the permeation of large or charged solutes can induce large deformations in the bilayer.[12,49,51−53] The solubility−diffusion model describes permeation as a flux along z, so the bilayer environment is assumed to be largely homogeneous at a given depth. The canonical solubility−diffusion model is generally invalid when permeation involves a large deformation of the bilayer or the partial hydration of the solute inside the membrane. In these situations, the solute will experience a range of dynamical environments at a given depth, and the deformation and hydration processes are likely to occur on a slower time scale than the flux along the z-axis. Enhanced sampling methods have been developed to ensure that orthogonal degrees of freedom are correctly sampled when calculating the potential of mean force along z,[50,54] although a rigorous model for the calculation of permeability coefficients will also require including the effects of these additional degrees of freedom on the dynamics of permeation. Some progress toward this has already been made by Parisio et al.[55] and Comer et al.,[17] who presented strategies for including the effect of solute orientation in the calculation of permeability.

A subsequent paper by Comer et al. noted that the calculated diffusivity of a water molecule at the center of a POPC bilayer was sensitive to the time delay of their Bayesian analyses method.[48] They attributed this to solute experiencing multiple kinetic regimes at a given position in the bilayer. The possibility of multiple kinetic regimes is not considered in the solubility−diffusion model, so a revised model for permeation would need to be developed to comprehensively address these issues. Nevertheless, the solubility−diffusion model combined with GLE methods for calculating diffusivity is a simple and computationally tractable method that is able to predict permeabilities with reasonable accuracy with respect to that achieved experimentally.[8,24]

CONCLUSIONS

Two methods based on the generalized Langevin equation were examined for their utility in calculating transmembrane diffusivity profiles. The first method uses the PACF of a solute harmonically restrained at a chosen bilayer depth, while the second method uses the VACF of the solute. The VACF method requires that the diffusivity be extrapolated from an equation involving the Laplace transform of the VACF, so an algorithm was developed to calculate solute diffusivity automatically using this method.

These methods were tested by calculating the diffusivity of solutes in bulk liquids. The VACF method predicted diffusivities that were in closer agreement with the reference Einstein relation than those from the PACF method and had a smaller standard error. The PACF method was also more sensitive to the use of a stochastic thermostat, so this method should be used only with thermostats that have a small effect on transport properties. On the other hand, the PACF method was less sensitive to the spring constant chosen for the harmonic restraining force. Generally, the VACF method should be used cautiously, and checks should be performed to ensure the extrapolation technique is accurate for a given simulation.

The calculation of a well-defined value for $D(z)$ for the permeation of a solute across a membrane is inherently challenging due to the complex dynamics of the bilayer. The methods predicted significantly different diffusivity profiles for a water molecule permeating a DPPC lipid bilayer. When the solute is immersed in the bilayer, the PACF can decay slowly due to long time scale fluctuations. This spuriously lowers the calculated diffusion coefficients, particularly at the lipid−water interface and the upper regions of the lipid tails. In contrast, the VACF decays quickly at all bilayer depths, so it is not affected by these long time scale fluctuations. The intramembrane diffusion coefficients calculated using the VACF method are systematically higher than those calculated using the PACF method. A comparison of the diffusion rate at the center of the bilayer calculated using the distribution of displacements from unrestrained simulations found that the VACF method overestimates the diffusivity by roughly 15%, but the PACF method underestimates the diffusivity by roughly 50%. These GLE methods should be used cautiously when calculating transmembrane diffusivity profiles, and there are opportunities for further development and application of new methods that resolve these issues.[15−18]

DOI: 10.1021/acs.jctc.6b00747
J. Chem. Theory Comput. 2016, 12, 5609−5619

APPENDIX A: DERIVATION OF EXPRESSION FOR $D(S)$ FROM THE GLE

The generalized Langevin equation (GLE) for the motion of a one-dimensional harmonic oscillator in a frictional bath along the z-axis is

$$m\ddot{z}(t) = -kz(t) - \int_0^t \dot{z}(\tau)\zeta(t-\tau)\mathrm{d}\tau + R(t) \tag{9}$$

where k is the spring constant of the restraining harmonic potential, $\zeta(t)$ is dynamic friction kernel, and $R(t)$ is the random force. To derive an expression for the diffusion coefficient of the solute, we multiply eq 9 through by $\dot{z}(0)$ (i.e., initial velocity):

$$m\dot{z}(0)\ddot{z}(t) = -\dot{z}(0)kz(t) - \int_0^t \dot{z}(0)\dot{z}(\tau)\zeta(t-\tau)\mathrm{d}\tau + R(t)\dot{z}(0) \tag{10}$$

This equation can be restated so that it is only in terms of $\dot{z}$ by replacing $z(t)$ with an integral of $\dot{z}(t)$ and noting that $\ddot{z}(t) = \frac{\mathrm{d}}{\mathrm{d}t}\dot{z}(t)$

$$m\dot{z}(0)\frac{\mathrm{d}}{\mathrm{d}t}\dot{z}(t) = -k\dot{z}(0)\int_0^t \dot{z}(t)\mathrm{d}t - \int_0^t \dot{z}(0)\dot{z}(\tau)\zeta(t-\tau)\mathrm{d}\tau + R(t)\dot{z}(0) \tag{11}$$

By taking the ensemble average of this equation, we obtain

$$m\frac{\mathrm{d}}{\mathrm{d}t}\langle\dot{z}(0)\dot{z}(t)\rangle = -k\int_0^t \langle\dot{z}(0)\dot{z}(t)\rangle\mathrm{d}t - \int_0^t \langle\dot{z}(0)\dot{z}(\tau)\rangle\zeta(t-\tau)\mathrm{d}\tau + \langle R(t)\dot{z}(0)\rangle \tag{12}$$

This equation can be immediately simplified in two ways: (i) the product of the random force and initial velocity will average to zero (i.e., $\langle R(t)\dot{z}(0)\rangle = 0$) and (ii) the VACF is defined as $C_v(t) = \langle\dot{z}(0)\dot{z}(t)\rangle$; thus, eq 12 becomes

$$m\frac{\mathrm{d}}{\mathrm{d}t}C_v(t) = -k\int_0^t C_v(t)\mathrm{d}t - \int_0^t C_v(t)\zeta(t-\tau)\mathrm{d}\tau \tag{13}$$

The Laplace transform of this equation gives

$$m\mathcal{L}\left\{\frac{\mathrm{d}}{\mathrm{d}t}C_v(t)\right\} = -k\mathcal{L}\left\{\int_0^t C_v(t)\mathrm{d}t\right\} - \mathcal{L}\left\{\int_0^t C_v(t)\zeta(t-\tau)\mathrm{d}\tau\right\} \tag{14}$$

Taking advantage of some Laplace transform identities, this equation simplifies to

$$m[s\hat{C}_v(s) - C_v(0)] = -k\frac{1}{s}\hat{C}_v(s) - \hat{C}_v(s)\hat{\zeta}(s) \tag{15}$$

where $\hat{C}_v = \mathcal{L}\{C_v\}$. Rearranging this equation to solve for $\hat{\zeta}$, we arrive at

$$\hat{\zeta}(s) = \frac{-m[s\hat{C}_v(s) - C_v(0)] - \frac{k}{s}\hat{C}_v(s)}{\hat{C}_v(s)} \tag{16}$$

We can then take the reciprocal of the above expression and multiply by k_BT:

$$\frac{k_BT}{\hat{\zeta}(s)} = \frac{-\hat{C}_v(s)k_BT}{m[s\hat{C}_v(s) - C_v(0)] + \frac{k}{s}\hat{C}_v(s)} \tag{17}$$

The diffusion coefficient of the solute, D, can be related to ζ using the Stokes–Einstein equation, $D = \frac{k_BT}{\zeta}$, and taking the limit as s approaches 0:

$$D = \lim_{s\to 0}\frac{k_BT}{\hat{\zeta}(s)} = \lim_{s\to 0}\frac{-\hat{C}_v(s)k_BT}{m[s\hat{C}_v(s) - C_v(0)] + \frac{k}{s}\hat{C}_v(s)} \tag{18}$$

This equation can be simplified further using the following identities: $C_v(0) = \langle\dot{z}(0)\dot{z}(0)\rangle = \langle\dot{z}^2\rangle$; $k = \frac{k_BT}{\langle z^2\rangle}$; $m = \frac{k_BT}{\langle\dot{z}^2\rangle}$. Using these relations, eq 18 becomes

$$D(s) = \lim_{s\to 0}\frac{-\hat{C}_v(s)\langle\dot{z}^2\rangle\langle z^2\rangle}{\hat{C}_v(s)\left[s\langle z^2\rangle + \frac{1}{s}\langle\dot{z}^2\rangle\right] - \langle\dot{z}^2\rangle\langle z^2\rangle} \tag{19}$$

This limit cannot be taken directly because of the $1/s$ term in the denominator. However, Hummer derived an alternative expression by replacing $\hat{C}_v(s)$ with $\hat{C}_z(s)$.[15] The VACF is equal to the derivative of the correlation function of the displacement (δz) at times t and t':[56]

$$\langle\dot{z}(0)\dot{z}(t)\rangle = \frac{\partial^2}{\partial t\partial t'}\langle\delta z(t)\delta z(t')\rangle \tag{20}$$

Rewriting the function to be in terms of t and the time difference $t'-t$, the VACF can be expressed as the second derivative of the PACF:

$$\langle\dot{z}(0)\dot{z}(t)\rangle = \frac{\partial^2}{\partial t\partial t'}\langle\delta z(0)\delta z(t-t')\rangle \tag{21}$$

$$= -\frac{\partial^2}{\partial t^2}\langle\delta z(0)\delta z(t-t')\rangle \tag{22}$$

In terms of the correlation functions, this gives us

$$C_v(t) = -\frac{\partial^2}{\partial t^2}C_z(t) \tag{23}$$

The Laplace transform of this equation gives

$$\hat{C}_v(t) = s\hat{C}_z(0) - s^2\hat{C}_z(t) \tag{24}$$

Noting that $\hat{C}_z(0) = \langle z^2\rangle$, substituting this expression into eq 19 gives

$$D(s) = \lim_{s\to 0}\frac{-[s\langle z^2\rangle - s^2\hat{C}_z(s)]\langle\dot{z}^2\rangle\langle z^2\rangle}{[s\langle z^2\rangle - s^2\hat{C}_z(s)]\left[s\langle z^2\rangle + \frac{1}{s}\langle\dot{z}^2\rangle\right] - \langle\dot{z}^2\rangle\langle z^2\rangle} \tag{25}$$

This can be simplified to

$$D(s) = \lim_{s\to 0}\frac{\langle\dot{z}^2\rangle\langle z^2\rangle[\langle z^2\rangle - s\hat{C}_z(s)]}{\hat{C}_z(s)[s^2\langle z^2\rangle + \langle\dot{z}^2\rangle] - s\langle\dot{z}^2\rangle^2} \tag{26}$$

The limit of this equation can be taken directly, noting that $\lim_{s\to 0}\hat{C}_z(s) = \int_0^\infty C_z(t)\mathrm{d}t$:

$$D = \frac{\mathrm{var}(z)^2}{\int_0^\infty C_z(t)\mathrm{d}t} \tag{27}$$

DOI: 10.1021/acs.jctc.6b00747
J. Chem. Theory Comput. 2016, 12, 5609−5619

APPENDIX B: DESCRIPTION OF $D(S)$ EXTRAPOLATION METHOD

The calculation of the diffusion coefficient of the solute from the velocity autocorrelation function requires a numerical solution to the equation

$$D(z_i = \langle z \rangle_i) = \lim_{s \to 0} \frac{-\hat{C}_v(s; z_i)\langle \delta z^2 \rangle_i \langle \dot{z}^2 \rangle_i}{\hat{C}_v(s; z_i)[s\langle \delta z^2 \rangle_i + \langle \dot{z} \rangle_i / s] - \langle \delta z^2 \rangle_i \langle \dot{z}^2 \rangle_i} \quad (28)$$

The singularity at $s = 0$ requires that the value of $D(s = 0)$ be extrapolated numerically from an interval of the equation that is well-behaved. This interval lies between the second and third singularities of $D(s)$, denoted s_1 and s_2.

To identify the locations of s_1 and s_2, the roots of the denominator of eq 3 are found numerically. This process is illustrated in Figure 10. The method first finds the location of

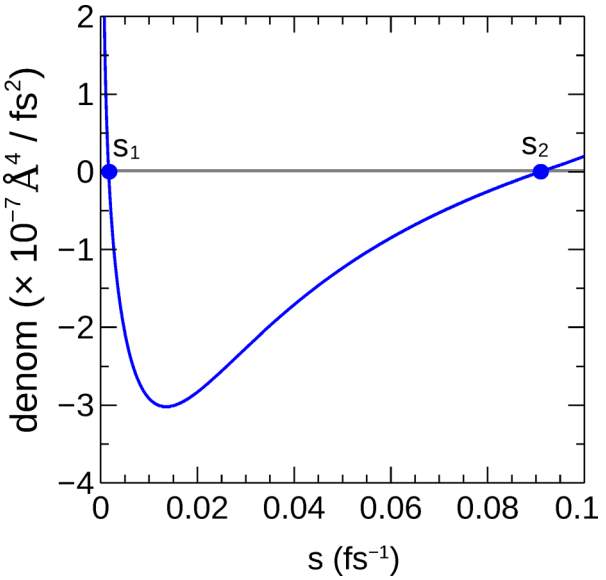

Figure 10. Denominator of eq 3 for a harmonically restrained water molecule in a simulation cell of liquid water (TIP3P model, k = 10 kcal mol^{-1} Å^{-2}). The second and third singularities of $D(s)$ (s_1 and s_2, respectively) are identified by finding the roots in this equation.

the minimum of the denominator, $s_{min,denom}$, using Brent's method.[57] s_1 and s_2 are located numerically using Tom's 748 method[58] to find the roots in the $[0.00001, s_{min,denom}]$ and $[s_{min,denom}, 1]$ intervals, respectively. The minimum of $D(s)$ (s_{min}) in the $[s_1, s_2]$ interval is then found using Brent's method.

A region of low curvature in $D(s)$ is found by calculating the second derivative of $D(s)$ over the interval $[s_{min}, s_2]$ by two iterations of numerical differentiation. A smoothing algorithm is applied at each iteration to reduce the effect of numerical error. The position of minimum curvature in $D(s)$ is then identified by a numerical search. The value of $D(s = 0)$ is extrapolated from this section of the curve by a linearization of $D(s)$.

The direct linear extrapolation of $D(s = 0)$ from a line tangent to the position of minimum curvature is very sensitive to numerical error. To improve the numerical stability of the extrapolation, a segment with low curvature is extended around the point of minimum curvature. This segment of the curve is fit to a linear equation using least-squares regression analysis. $D(s = 0)$ is determined from the y-intercept of this linear approximation of $D(s)$. The coefficient of determination from this fit (R^2) is an indicator of the appropriateness of linear extrapolation of $D(s)$. For the extrapolation of $D(s = 0)$ in the VACF calculations of diffusivity in the homogeneous systems, R^2 was greater than 0.99 for the linear fit of the curve segment used for extrapolation.

This method relies on the effective linear extrapolation of $D(s)$ to the y-intercept. A segment where the curvature is low is essential for an accurate extrapolation. The researcher should plot $D(s)$ to ensure the function has a nearly linear segment between the singularities.

ASSOCIATED CONTENT

Supporting Information

The Supporting Information is available free of charge on the ACS Publications website at DOI: 10.1021/acs.jctc.6b00747.

Sample input files for NAMD and GROMACS simulations, nonaveraged diffusivity profiles, and correlation functions for simulations near the lipid−water interface (PDF)

AUTHOR INFORMATION

Corresponding Author

*E-mail: crowley@mun.ca.

Funding

The authors thank NSERC of Canada for funding through the Discovery Grant program (Application 418505-2012). E.A.W. and K.G. thank Memorial University for graduate fellowships. E.A.W. also thanks ACENET for an Advanced Research Computing Fellowship. Computational resources were provided by Compute Canada (RAPI: djk-615-ab) through the Calcul Quebec and ACENET consortia.

Notes

The authors declare no competing financial interest.

REFERENCES

(1) Copeland, R. A.; Pompliano, D. L.; Meek, T. D. Drug-Target Residence Time and its Implications for Lead Optimization. *Nat. Rev. Drug Discovery* **2006**, *5*, 730−739.

(2) Lu, H.; Tonge, P. J. Drug-target Residence Time: Critical Information for Lead Optimization. *Curr. Opin. Chem. Biol.* **2010**, *14*, 467−474.

(3) Stein, W.; Lieb, W. *Transport and Diffusion Across Cell Membranes*; Academic Press, 1986.

(4) Di, L.; Kerns, E. H.; Fan, K.; McConnell, O. J.; Carter, G. T. High Throughput Artificial Membrane Permeability Assay for Blood-Brain Barrier. *Eur. J. Med. Chem.* **2003**, *38*, 223−232.

(5) Diamond, J. M.; Katz, Y. Interpretation of Nonelectrolyte Partition Coefficients Between Dimyristoyl Lecithin and Water. *J. Membr. Biol.* **1974**, *17*, 121−154.

(6) Marrink, S. J.; Berendsen, H. J. C. Simulation of Water Transport Through a Lipid Membrane. *J. Phys. Chem.* **1994**, *98*, 4155−4168.

(7) Marrink, S. J.; Berendsen, H. J. C. Permeation Process of Small Molecules across Lipid Membranes Studied by Molecular Dynamics Simulations. *J. Phys. Chem.* **1996**, *100*, 16729−16738.

(8) Lee, C. T.; Comer, J.; Herndon, C.; Leung, N.; Pavlova, A.; Swift, R. V.; Tung, C.; Rowley, C. N.; Amaro, R. E.; Chipot, C.; Wang, Y.; Gumbart, J. C. Simulation-Based Approaches for Determining Membrane Permeability of Small Compounds. *J. Chem. Inf. Model.* **2016**, *56*, 721−733.

(9) Awoonor-Williams, E.; Rowley, C. N. Molecular Simulation of Nonfacilitated Membrane Permeation. *Biochim. Biophys. Acta, Biomembr.* **2016**, *1858*, 1672−1687.

DOI: 10.1021/acs.jctc.6b00747
J. Chem. Theory Comput. 2016, 12, 5609−5619

(10) Hub, J. S.; de Groot, B. L.; van der Spoel, D. g_wham − A Free Weighted Histogram Analysis Implementation Including Robust Error and Autocorrelation Estimates. *J. Chem. Theory Comput.* **2010**, *6*, 3713−3720.
(11) Wennberg, C. L.; van der Spoel, D.; Hub, J. S. Large Influence of Cholesterol on Solute Partitioning into Lipid Membranes. *J. Am. Chem. Soc.* **2012**, *134*, 5351−5361.
(12) Neale, C.; Pomès, R. Sampling Errors in Free Energy Simulations of Small Molecules in Lipid Bilayers. *Biochim. Biophys. Acta, Biomembr.* **2016**, *1858*, 2539−2548.
(13) Einstein, A. Investigations on the Theory of the Brownian Movement. *Dover Books on Physics Series*; Dover Publications, 1956.
(14) Kubo, R. The Fluctuation-Dissipation Theorem. *Rep. Prog. Phys.* **1966**, *29*, 255.
(15) Hummer, G. Position-Dependent Diffusion Coefficients and Free Energies from Bayesian Analysis of Equilibrium and Replica Molecular Dynamics Simulations. *New J. Phys.* **2005**, *7*, 34−34.
(16) Krivov, S. V.; Karplus, M. Diffusive Reaction Dynamics on Invariant Free Energy Profiles. *Proc. Natl. Acad. Sci. U. S. A.* **2008**, *105*, 13841−13846.
(17) Comer, J.; Chipot, C.; González-Nilo, F. D. Calculating Position-Dependent Diffusivity in Biased Molecular Dynamics Simulations. *J. Chem. Theory Comput.* **2013**, *9*, 876−882.
(18) Mugnai, M. L.; Elber, R. Extracting the Diffusion Tensor from Molecular Dynamics Simulation with Milestoning. *J. Chem. Phys.* **2015**, *142*, 014105.
(19) Woolf, T. B.; Roux, B. Molecular Dynamics Simulation of the Gramicidin Channel in a Phospholipid Bilayer. *Proc. Natl. Acad. Sci. U. S. A.* **1994**, *91*, 11631−11635.
(20) Woolf, T. B.; Roux, B. Conformational Flexibility of o-Phosphorylcholine and o-Phosphorylethanolamine: A Molecular Dynamics Study of Solvation Effects. *J. Am. Chem. Soc.* **1994**, *116*, 5916−5926.
(21) Schumaker, M. F.; Pomès, R.; Roux, B. A Combined Molecular Dynamics and Diffusion Model of Single Proton Conduction through Gramicidin. *Biophys. J.* **2000**, *79*, 2840−2857.
(22) Bonhenry, D.; Tarek, M.; Dehez, F. Effects of Phospholipid Composition on the Transfer of a Small Cationic Peptide Across a Model Biological Membrane. *J. Chem. Theory Comput.* **2013**, *9*, 5675−5684.
(23) Carpenter, T. S.; Kirshner, D. A.; Lau, E. Y.; Wong, S. E.; Nilmeier, J. P.; Lightstone, F. C. A Method to Predict Blood-Brain Barrier Permeability of Drug-Like Compounds Using Molecular Dynamics Simulations. *Biophys. J.* **2014**, *107*, 630−641.
(24) Riahi, S.; Rowley, C. N. Why Can Hydrogen Sulfide Permeate Cell Membranes? *J. Am. Chem. Soc.* **2014**, *136*, 15111−15113.
(25) Tuckerman, M. E. Statistical Mechanics: Theory and Molecular Simulation. *Oxford Graduate Texts*; Oxford University Press: Oxford, 2010.
(26) Straub, J. E.; Borkovec, M.; Berne, B. J. Calculation of Dynamic Friction on Intramolecular Degrees of Freedom. *J. Phys. Chem.* **1987**, *91*, 4995−4998.
(27) Allen, M.; Tildesley, D. *Computer Simulation of Liquids*; Oxford Science Publications, Clarendon Press: Oxford, 1989; pp 185−190.
(28) Wiener, N. Generalized Harmonic Analysis. *Acta Mathematica* **1930**, *55*, 117−258.
(29) Khintchine, A. Korrelationstheorie der Stationären Stochastischen Prozesse. *Mathematische Annalen* **1934**, *109*, 604−615.
(30) Phillips, J. C.; Braun, R.; Wang, W.; Gumbart, J.; Tajkhorshid, E.; Villa, E.; Chipot, C.; Skeel, R. D.; Kalé, L.; Schulten, K. Scalable Molecular Dynamics with NAMD. *J. Comput. Chem.* **2005**, *26*, 1781−1802.
(31) Ryckaert, J.-P.; Ciccotti, G.; Berendsen, H. J. C. Numerical Integration of the Cartesian Equations of Motion of a System with Constraints: Molecular Dynamics of n-Alkanes. *J. Comput. Phys.* **1977**, *23*, 327−341.
(32) Darden, T.; York, D.; Pedersen, L. Particle Mesh Ewald: An N log(N) Method for Ewald Sums in Large Systems. *J. Chem. Phys.* **1993**, *98*, 10089−10092.
(33) Fischer, J.; Lago, S. Thermodynamic Perturbation Theory for Molecular Liquid Mixtures. *J. Chem. Phys.* **1983**, *78*, 5750−5758.
(34) Jorgensen, W. L.; Chandrasekhar, J.; Madura, J. D.; Impey, R. W.; Klein, M. L. Comparison of Simple Potential Functions for Simulating Liquid Water. *J. Chem. Phys.* **1983**, *79*, 926−935.
(35) MacKerell, A. D.; et al. All-Atom Empirical Potential for Molecular Modeling and Dynamics Studies of Proteins. *J. Phys. Chem. B* **1998**, *102*, 3586−3616.
(36) Vanommeslaeghe, K.; Hatcher, E.; Acharya, C.; Kundu, S.; Zhong, S.; Shim, J.; Darian, E.; Guvench, O.; Lopes, P.; Vorobyov, I.; Mackerell, A. D. CHARMM General Force Field: A Force Field for Drug-Like Molecules Compatible with the CHARMM All-Atom Additive Biological Force Fields. *J. Comput. Chem.* **2009**, *31*, 671−690.
(37) Klauda, J. B.; Venable, R. M.; Freites, J. A.; O'Connor, J. W.; Tobias, D. J.; Mondragon-Ramirez, C.; Vorobyov, I.; Alexander, D.; MacKerell, J.; Pastor, R. W. Update of the CHARMM All-Atom Additive Force Field for Lipids: Validation on Six Lipid Types. *J. Phys. Chem. B* **2010**, *114*, 7830−7843.
(38) Our preliminary calculations indicate that the diffusivity inside the bilayer calculated using GLE is also sensitive to the spring constant. Work to identify optimal spring constants is ongoing.
(39) Gaalswyk, K.; Rowley, C. N. ACFCalculator. https://github.com/RowleyGroup/ACFCalculator (accessed August 25, 2016).
(40) Schneider, T.; Stoll, E. Molecular-Dynamics Study of a Three-Dimensional One-Component Model for Distortive Phase Transitions. *Phys. Rev. B: Condens. Matter Mater. Phys.* **1978**, *17*, 1302−1322.
(41) Frenkel, D.; Smit, B. *Understanding Molecular Simulation*, 2nd ed.; Academic Press, Inc.: Orlando, FL, 2001.
(42) Basconi, J. E.; Shirts, M. R. Effects of Temperature Control Algorithms on Transport Properties and Kinetics in Molecular Dynamics Simulations. *J. Chem. Theory Comput.* **2013**, *9*, 2887−2899.
(43) The simulations using the Lowe−Anderson thermostat used the NAMD-default settings of a 2.7 Å distance cutoff and a collision rate of 50 ps^{-1}.
(44) Lowe, C. P. An Alternative Approach to Dissipative Particle Dynamics. *Europhys. Lett.* **1999**, *47*, 145.
(45) Koopman, E. A.; Lowe, C. P. Advantages of a Lowe−Andersen Thermostat in Molecular Dynamics Simulations. *J. Chem. Phys.* **2006**, *124*, 204103.
(46) We note that some related models, e.g., Caldeira−Leggetta, describe the system using a more complicated potential and can still be described using the GLE as the equation of motion.
(47) Mark, P.; Nilsson, L. Structure and Dynamics of the TIP3P, SPC, and SPC/E Water Models at 298 K. *J. Phys. Chem. A* **2001**, *105*, 9954−9960.
(48) Comer, J.; Schulten, K.; Chipot, C. Calculation of Lipid-Bilayer Permeabilities Using an Average Force. *J. Chem. Theory Comput.* **2014**, *10*, 554−564.
(49) Neale, C.; Bennett, W. D.; Tieleman, D. P.; Pomès, R. Statistical Convergence of Equilibrium Properties in Simulations of Molecular Solutes Embedded in Lipid Bilayers. *J. Chem. Theory Comput.* **2011**, *7*, 4175−4188.
(50) Neale, C.; Madill, C.; Rauscher, S.; Pomès, R. Accelerating Convergence in Molecular Dynamics Simulations of Solutes in Lipid Membranes by Conducting a Random Walk along the Bilayer Normal. *J. Chem. Theory Comput.* **2013**, *9*, 3686−3703.
(51) MacCallum, J. L.; Bennett, W. D.; Tieleman, D. P. Transfer of Arginine into Lipid Bilayers Is Nonadditive. *Biophys. J.* **2011**, *101*, 110−117.
(52) Li, L.; Vorobyov, I.; Allen, T. W. The Different Interactions of Lysine and Arginine Side Chains with Lipid Membranes. *J. Phys. Chem. B* **2013**, *117*, 11906−11920.
(53) Bennett, W. F. D.; Tieleman, D. P. The Importance of Membrane Defects - Lessons from Simulations. *Acc. Chem. Res.* **2014**, *47*, 2244−2251.
(54) Sun, R.; Dama, J. F.; Tan, J. S.; Rose, J. P.; Voth, G. A. Transition-Tempered Metadynamics is a Promising Tool for Studying

DOI: 10.1021/acs.jctc.6b00747
J. Chem. Theory Comput. 2016, 12, 5609−5619

the Permeation of Drug-like Molecules through Membranes. *J. Chem. Theory Comput.* **2016**, 1.
(55) Parisio, G.; Sperotto, M. M.; Ferrarini, A. Flip-Flop of Steroids in Phospholipid Bilayers: Effects of the Chemical Structure on Transbilayer Diffusion. *J. Am. Chem. Soc.* **2012**, *134*, 12198−12208.
(56) Doi, M. *Soft Matter Physics*; Oxford University Press: Oxford, 2013.
(57) Brent, R. P. An Algorithm with Guaranteed Convergence for Finding a Zero of a Function. *Comput. J.* **1971**, *14*, 422−425.
(58) Alefeld, G. E.; Potra, F. A.; Shi, Y. Algorithm 748: Enclosing Zeros of Continuous Functions. *ACM Trans. Math. Softw.* **1995**, *21*, 327−344.

DOI: 10.1021/acs.jctc.6b00747
J. Chem. Theory Comput. 2016, 12, 5609−5619